Computational Aspects of Single Molecule Kinetics for Coupled Catalytic Cycles: A Spectral Analysis

Suming An¹, Prajay Patel², Cong Liu*², and Rex T. Skodje*¹

- 1) Department of Chemistry, University of Colorado, Boulder, CO 80309
- 2) Chemical Sciences and Engineering Division, Argonne National Laboratory, Lemont,

IL 60639

Abstract:

Catalysis from single active sites is analyzed using methods developed from single molecule kinetics. Using a stochastic Markov state description, the observable properties of general catalytic networks of reactions are expressed using an eigenvalue decomposition of the transition matrix for the Markov process. By the use of a sensitivity analysis, the necessary eigenvalues and eigenvectors are related to the energies of controlling barriers and wells located along the reaction routes. A generalization of the energetic span theory allows the eigenvalues to be computed from several activation energies corresponding to distinct barrier-well pairings. The formalism is demonstrated for model problems and for a physically realistic mechanism for an alkene hydrogenation reaction on a single atom catalyst. The spectral analysis permits a hierarchy of timescales to identified from the single molecule signal which correspond to specific relaxation modes in the network.

I. Introduction

Computational methods have become increasingly essential in the study of heterogeneous catalysis. In particular, the use of density functional theory (DFT) for the potential energy surface (PES) in concert with transition state theory (TST) for kinetic rates has made it possible to understand the detailed chemistry of a number of important processes. ¹⁻⁴ These theoretical tools assist in the elucidation of the underlying atomic mechanism and can help in the design and optimization of the catalyst itself. While the DFT modeling of modestly sized mechanisms is tractable kinetics on perfect crystal faces, problems exhibiting disordered catalytically active sites can require extremely burdensome numbers of calculations. As an example, consider the important case of single atom catalysts (SAC) where a diverse range of local environments of the catalytic atom may strongly affect its activity. ^{5 6} For atoms anchored to disordered supports, the number of distinct PES required to represent the mechanism can be extremely large. ^{7 8} The local environment

of the SAC not only influences the rate coefficients of the catalytic mechanism but potentially also catalytic pathway itself.⁹ In this work, we explore some new methods to understand and predict how catalytic observables respond to the energetic features in complex reaction networks. This may greatly reduce the number of required calculations required to describe a catalytic process. If certain key reaction steps are identified, it is possible to reduce the extensive modeling to such essential reactions. Also, if the local environment is described by a set of structural parameters, it might be possible to restrict the DFT calculations to certain optimal parameter ranges that most strongly contribute to observed chemistry.

The most common observables modeled in theoretical studies of catalysts are bulk quantities such as the turnover frequency (TOF) and product selectivity which average over sites. We have recently suggested¹⁰ that microscopic level methods inspired by single molecule kinetics (SMK)¹¹⁻¹⁴ are of use for the study of SAC. In SMK, one probes the catalytic turnover at a single site using spatially and temporally resolved measurements of reaction products or intermediates. These methods were first developed for enzymatic reactions in the case of Michaelis-Menten systems $E + S \leftrightarrow ES \rightarrow E + P$, where S is the substrate, P is the product, and E is the catalytic enzyme. 15 Real time measurements of turnover from a single enzyme molecule could then be characterized by a statistical probability distribution function (PDF) of turnover times. The turnover time, t, was identified by waiting times between product release steps measurable via the "on" and "off" intervals of a photolytic species and are represented by a normalized probability distribution f(t). The statistical properties of this distribution then provided insight into the mechanistic and conformational kinetics of the enzymatic reaction and significant progress has been made in the formal treatment of these systems. 16-26 Chen and coworkers, 27-32 and other groups³³⁻³⁶have taken the SMK technology into the realm of heterogeneous catalytic systems. Xu et al.37 developed a scheme to model turnover from a single nanoparticle using a Langmuir-Hinschelwood expression that makes use of a steady state approximation for the adsorptiondesorption kinetics. For SAC, the methods of SMK make it possible to interrogate the kinetics at single catalyst sites and to directly investigate the role of disorder. The underlying motivation of many SMK studies is to address the difficult inverse problem where the kinetic observation is used to deduce the underlying "hidden" mechanism. The SMK expands the range of observables to

include statistical fluctuations in the reaction that are not apparent in the highly averaged bulk experiments.

In a single molecule view of steady state catalysis, we consider the passage of a molecule through the network of transient chemical states occurring between sequential product release steps. This gives a different perspective on the kinetics than accrues from conventional bulk kinetics. Instead of focusing on the time evolution of species concentrations and their steady state limits, we attempt to model the waiting time between product release events occurring at a single catalytic site which is a product of the pathway experienced by a tagged molecule moving through the chemical network. The most efficient way of representing the kinetics employs the Markov state picture of a stochastic process. ^{25,38-40} The species concentrations are replaced with occupancy probabilities that evolve according to a system of first order differential equations from which we can extract the probability distribution function f(t) of waiting times from a given catalytic site. The waiting time PDF obtained by experiment or modeling has shown a wide variety of behaviors. The measured f(t) has been represented by a sum of exponentials, stretched exponentials, ⁴¹ gamma distributions, ¹⁹ or even power law expressions. ⁴² We have found that in some cases f(t) may even show bimodal behavior. 10 It is common to characterize the PDF using moments, $\langle t^n \rangle$. The first moment is the mean first passage time through the network and gives a TOF that is identical to the bulk quantity if all sites are identical, i.e.

$$\nu = \frac{1}{\langle t \rangle} \tag{1.1}$$

The first two moments of f(t) are often combined into the randomness parameter, r,

$$r = \frac{\langle t^2 \rangle - \langle t \rangle^2}{\langle t \rangle^2} \tag{1.2}$$

that measures the deviation of the kinetics from pure Poisson statistics ($r_{poisson}=1$). The behavior of r versus substrate concentration for various catalytic motifs has been the subject of considerable interest, and several closely related analytical expressions have been proposed for r([S]). ¹⁶ ¹⁷ ²¹ ⁴³ ⁴⁶ The value observed for r constrains the complexity of the model required to model the kinetics in terms of the minimal number of intermediate states (>1/r), the number of transition states (>1/r), or the need for branching reaction pathways (r>1).

In the present work, we explore the behavior of the SMK observables from the standpoint of computational chemistry. Thus, we compute the free energy for stationary structures, i.e., barriers and wells, using quantum chemistry which then immediately yield rate coefficients from TST. The usual mechanism improvement strategy is to identify the key controlling reaction steps which are then calculated at a higher level to improve the performance of the model. However, it becomes difficult to identify the controlling energetic structures when the mechanism is complex or when disorder requires very large numbers of independent DFT calculations. Furthermore, passage through the catalytic network must necessarily involve sequences of elementary steps, i.e., chemical pathways, that induce simultaneous sensitivities to distant parts of the mechanism. 47 48 We show that a spectral decomposition of a stochastic transition matrix allows the sensitivities to be much easier understood. The eigenvalue spectrum is found as continuous functions of the controllable variables such as concentration, temperature, and disorder parameters. The behavior of the f(t) and its moments versus these parameters then assume a transparent mathematical meaning. For example, maxima and minima in r are related to avoided crossings of the eigenvalues. The eigenvalues themselves are accurately represented in terms of the energetics along specific pathways embedded in the chemical network. ⁴⁹ Those pathways are found by a local sensitivity analysis 50 51 and are consistent with traditional ideas in catalysis such as the energetic span theory⁵² and degree of reaction control.⁵³ Understanding these effects is important in strategies to design effective catalysts.⁵⁴

II. Theoretical Methods

A. Rate expressions

As a kinetic general framework, we imagine a SAC that can convert one or more substrate molecules (S) into product molecules (P) through a reaction network for an isolated SAC on a support surface. The catalytic network consists of N distinct chemical species, X_i , that carry the catalytic atom and may consist of a bare catalytic site, a catalytic site with ligands attached, or any intermediates involving chemically altered molecules attached to the SAC. These species interconvert via the pseudo-first-order reactions, $X_j(+Z) \rightarrow X_i$ with rates given $k_{i,j}[X_j]$ where the concentration of any substrate or inhibitor, Z, is assumed to be nearly constant in time and is absorbed into $k_{i,j}$. The rate expressions for the reaction step $j \rightarrow i$ is given by the Eyring form,

$$k_{i,j} = \frac{k_B T}{h} e^{-\frac{\Delta G_{i,j}^{\ddagger,0}}{k_B T}} \cdot Z$$
 (2.1)

where Z is either 1 or a concentration of a substrate or inhibitor depending on the reaction and $\Delta G_{i,j}^{\pm,0}$ is the standard free energy barrier for the reaction $X_j(+Z) \to X_i$. The free energies are provided by quantum chemistry which are computed including entropic effects. It is important to emphasize that just one of the X_i -species can be occupied at a given time on a given SAC. In Michaelis-Menten kinetics⁵⁵ this would correspond to the conservation of catalyst, $E_0=[E]+[ES]$. Thus, we can convert the concentrations $[X_j]$ to "state" probabilities normalized to unity, i.e., the probability of species X_i being occupied is P_j with $\sum_j^N P_j = 1$. The rate coefficients, $k_{i,j}$ are interpreted as the transition probability per unit time between state j and state i, i.e., $j \underset{k_{i,j}}{\longrightarrow} i$. This is the conventional Markov state model⁵⁶ often employed for enzymatic kinetics although more general formulations are possible.²³ Finally, we note that in a disordered system the free energies and thus the rate coefficients can depend on the particular site that this being probed. We shall assume this site dependence can be modeled using a small number of continuous structural parameters that characterize the local environment of the SAC. These parameter dependencies are obtained from the quantum chemistry calculations.

B. Kinetic Model

We are interested in the steady-state kinetics of a catalytic network described a network of pseudo-first-order processes. Recapitulating the method presented in ref. 10, we compute the state occupancy probabilities $P_i(t)$ from time-evolution equations including all sources and sinks within the network. The state probabilities evolve by the N first-order ordinary differential equations eq. (2.2) using the probability vector $\mathbf{P}^T = (P_1, \dots, P_N)$ and the $N \times N$ rate generating matrix \mathbf{G} are

$$\frac{d\mathbf{P}(t)}{dt} = \mathbf{G} \cdot \mathbf{P}(t) \tag{2.2}$$

and

$$\mathbf{G} = \begin{pmatrix} -k_1 & \dots & k_{1,N} \\ \vdots & \ddots & \vdots \\ k_{N,1} & \dots & -k_N \end{pmatrix}$$
 (2.3)

The diagonal elements $G_{i,i}$ for i=1,...,N are the negative decay probabilities per unit time of state i, $k_i = \sum_{j \neq i}^{N} k_{j,i}$. In steady state, eq. (2.2) is $\mathbf{G} \cdot \mathbf{P}_{ss} = 0$ which can be solved using the constraint $\sum_{i} P_{ss,i} = \mathbf{1}^{T} \cdot \mathbf{P}_{ss} = 1$ where **1** is the N-vector of 1's. For any initial state $\mathbf{P}(0)$, $\mathbf{P}(t)$ will approach P_{ss} at long times assuming the rate coefficients are static. The eq. (2.2) can be written in a form more appropriate to a single molecule experiment to obtain waiting times. We imagine an experiment designed to reveal the waiting time t corresponding to the interval between successive product release events. Thus, a SAC releases a product at time 0, which starts the clock for the next cycle ending in the release of another product at a time t. There can be one or more release reactions in the mechanism involving different reactions and different products. We make the important restriction that the product forming reactions are effectively irreversible corresponding to the initial rate, i.e the product concentration is zero. The "initial Markov state" following an observed product formation event is one of the species formed by these irreversible steps and we call that collection of states the "active sites", AS's. Many problems have just a single AS, but we will assume that m such AS in the network exists. The conversion between different AS can model non-renewal processes since a sequence of turnovers are not IID's, i.e., independent and identically distributed random variables.^{23 57 58} For convenience, we label the active sites i=1,...,m. All the transition rates into the m AS's are collected into a matrix τ , which we term the absorption matrix that has nonzero elements only for the one way transitions into the AS,

$$\boldsymbol{\tau}_{N\times N} = \begin{pmatrix} k_{1,1} & \cdots & k_{1,N} \\ \vdots & \ddots & \vdots \\ k_{m,1} & \cdots & k_{m,N} \\ 0 & \cdots & 0 \\ \vdots & \ddots & \vdots \\ 0 & \cdots & 0 \end{pmatrix}$$
 (2.4)

We can also define N×1 absorption vectors, τ_i , with i=1,...,m, that describe transitions into one specific AS i via $\tau_i = (k_{i,1} \dots k_{i,N})^T$ and which combine to form $\tau_{N\times N}$. In most cases, the absorption matrix will contain only a few nonzero elements.

As we discussed previously, 10 the continuous time Markov chain model theory permits a matrix T to be defined restricted to transitions between transient states that determine the properties of the single molecular experiment. The N×N matrix T is identical to G except that the transitions to the active sites are subtracted, i.e.,

$$T = G - \tau \tag{2.5}$$

A single molecule experiment involves measuring the distribution of waiting times between successive product measurements. This corresponds to the passage time from an active site through the network to any final active site which is treated as an absorbing state. It was shown¹⁰ that the PDF f(t) can be written as

$$f(t) = \mathbf{1}^{T} \cdot (-T) \cdot \exp(Tt) \cdot P(0)$$
(2.6)

and the moments of the PDF are given by

$$\langle t^n \rangle = n! \, \mathbf{1}^T \cdot (-\mathbf{T})^{-n} \cdot \mathbf{P}(0) \tag{2.7}$$

The turnover frequency of the SAC is thus given by

$$\nu = \frac{1}{\langle t \rangle} = \frac{1}{\mathbf{1}^T \cdot (-T)^{-1} \cdot \mathbf{P}(0)}$$
 (2.8)

We note that the initial probability vector P(0) corresponds to the steady state distribution of AS developed after many turnover events. It is given by the projection of P_{ss} onto the AS and is normalized to unity, i.e., $\mathbf{1}^T \cdot P(0) = 1$. Often P(0) is often just 1 for a single AS.

C. Analytical Expressions

A great deal has been learned by studying specific catalytic scenarios using analytical models of how the TOF or randomness parameters respond to changes in substrate concentration or other controllable variables. The most commonly studied catalytic motif is the linear chain shown in Fig. 1a which involves a single pathway and a single AS. The TOF for this special case was first deduced by Christensen⁵⁹ in 1953 and has been written in various forms since then. For future convenience, we give the inverse TOF expression for a chain of length N as

$$\langle t \rangle = \frac{1}{r_N} + \left(\frac{b_N}{r_{N-1} \cdot r_N} + \frac{1}{r_{N-1}}\right) + \left(\frac{b_{N-2} \cdot b_{N-1}}{r_{N-2} \cdot r_{N-1} \cdot r_N} + \frac{b_{N-2}}{r_{N-2} \cdot r_{N-1}} + \frac{1}{r_{N-2}}\right) + \cdots$$

$$+\left(\frac{b_{1}\cdot b_{2}\cdot ...\cdot b_{N-2}\cdot b_{N-1}}{r_{1}\cdot r_{2}\cdot ...\cdot r_{N-1}\cdot r_{N}} + \frac{b_{1}\cdot b_{2}\cdot ...\cdot b_{N-2}}{r_{1}\cdot r_{2}\cdot ...\cdot r_{N-1}} + \cdots + \frac{b_{1}}{r_{1}\cdot r_{2}} + \frac{1}{r_{1}}\right)$$
(2.9)

In eq. (2.9) we define r_j as the forward rate of reaction j and b_j as the backward rate of reaction j. We emphasize that there are no terms involving b_N since the final product step is assumed to be irreversible. The substrate concentrations enter as multiples of the appropriate forward rate but not the reverse reaction. The concentration dependence for linear cycles with any number of substrates can be expressed analytically using eq. (2.9). The usual TOF expression for the Michaelis Menten scheme $(E + S \underset{k_{\pm 1}}{\longleftrightarrow} ES \underset{k_2}{\to} E + P$) fits N=2 case with $K_M = \frac{k_{-1} + k_2}{k_1}$ and

$$v^{MM} = \frac{k_2 \cdot S}{S + K_M} \tag{2.10}$$

If two substrates are added sequentially, ⁶⁰ the general form of the TOF is

$$v^{TwoSub} = \frac{a \cdot S_1 S_2}{S_1 S_2 + b \cdot S_1 + c \cdot S_2 + d}$$
 (2.11)

where the coefficients a-d can be read off from eq. (2.9).

The randomness parameter is more complicated to express than the TOF, although it is possible to obtain a closed form expression for linear cycles.²¹ For the MM case, one has

$$r^{MM} = \frac{(S + K_M)^2 - 2\left(\frac{k_2}{k_1}\right)S}{(S + K_M)^2 + 2\left(\frac{k_2}{k_1}\right)S} \le 1$$
 (2.12)

For this simple example, a fit of (v, r_{RAN}) as functions of S provides a complete characterization of the full steady state kinetics. The analytical formula for the randomness parameter becomes quite a bit more complex for longer linear cycles. However, concentration dependence for one substrate can be shown to take the form

$$r = \frac{d_1 \left(\frac{S}{d_5}\right)^2 + 2d_2 \left(\frac{S}{d_5}\right) + d_3}{d_1 d_3 \left[1 + \left(\frac{S}{d_5}\right)\right]^2}$$
(2.13)

where d_1 - d_5 are elaborate, but known, functions of the rate coefficients $k_{i,j}$ for the nearest neighbor transitions. Unfortunately, this impressive expression often breaks down for multiple pathway reactions involving inhibitors and co-catalysts. It has been found that always $r \le 1$ for linear path problems, regardless of the concentration of substrate or number of intermediates. If the full

catalytic cycle were a pure Poisson process, then r=1 since $\langle t^2 \rangle = \langle t \rangle^2$. The minimum value of r places limits on the number of states or TS's in the cycle which correspond to multiple exponentials in the waiting time distribution f(t). A common case to find $r_{min}=1/2$ which corresponds to two equivalent TS's occurring along the reaction path.

D. Energy Picture

Our primary focus here is to relate the behavior of the single molecule observables to quantities obtained by a computational approach to catalysis. The computed free energies along the reaction network are inputs into the rate coefficients which then are used to model the kinetics. For single pathway catalytic cycles, the energetic span model suggested by Amatore and Jutand⁶¹ and improved by Kozuch and Shaik⁶²⁻⁶⁴ provides a useful guide to approximating the solution to eq. (2.9). The energetic span identifies two key structures, one TS and one INT, whose free energy difference defines a maximum energy span. To emphasize a distinction from the terminology of Kozuch and Shaik, since we are specializing to a case when the final step is irreversible, the highest transition state, called HTS, and the lowest intermediate, called LINT, are identified. This pair is chosen to maximize the energy of activation, $\Delta G_a = \Delta G_{HTS} - \Delta G_{LINT}$, subject to the constraint that LINT must lie before the HTS. Approximating the expression eq. (2.9) for the case when LINT and HTS are unique, we have

$$v_{span} \approx \frac{k_B T}{h} exp \left[-\frac{(\Delta G_{HTS} - \Delta G_{LINT})}{kT} \right]$$
 (2.14)

When there are two energetically equal HTS's along the path, it is clear that the TOF is then ½ its value for a single HTS. Similarly, if there are two energetically equivalent LINT's along the path we get ½ the TOF obtained with a single LINT.

We point out that the concentration of a substrate, co-catalyst, or inhibitor, "X", can be included in this picture by including the affinity in the free energy

$$\Delta G = \Delta G^0 - k_B T \cdot ln\left(\frac{[X]}{[X_0]}\right) \tag{2.15}$$

From eq. (2.15) we see that we can effectively "adjust" the barrier height of X-addition steps by changing [X]. For the simple MM mechanism, e.g., altering the substrate concentration [S] changes the free energy for the addition step E+S \rightarrow ES. Interestingly, the minimum of r, eq. (2.12),

occurs near the point where $\Delta G_{TS1}^0 - k_B T \cdot ln\left(\frac{[S]}{[S_0]}\right) = \Delta G_{TS2}^0$ which is where $[S] = K_M$.

Besides the HTS and LINT, the other barriers and wells along the linear path do not significantly affect the TOF except when they lie close in energy to the critical HTS or LINT. The standard free energies are obtained using quantum chemistry, and the energy span TOF requires only an accurate determination of two quantities, ΔG_{TS}^0 and ΔG_{INT}^0 rather than the 2N free energies along the route implicit in eq. (2.9). Once the HTS and LINT are identified, higher level QM calculations could be restricted to these structures.

Expression (2.14) will apply when a single pathway dominates the kinetics, even if the formal kinetic networks appear to be multiple branching. However, it is possible to generalize the energetic span idea to the case of two parallel simply coupled pathways as shown in Fig. 2a. To describe this case, we require three fundamental energies: the "left" and "right" highest TS's, HTSL and HTSR, and the lowest intermediate, LINT. As the name implies, the HTSL and HTSR are the highest barriers before two product producing reactions, and LINT is the lowest intermediate that is bracketed by HTSL and HTSR. The approximate TOF is thus

$$v_{span,parallel} \approx \frac{k_B T}{h} exp \left[-\frac{(MIN(\Delta G_{HTSL}, \Delta G_{HTSR}) - \Delta G_{LINT})}{kT} \right]$$
 (2.16)

E. Spectral analysis of the T-matrix

A useful way of understanding the behavior of the SMK is through the use of an eigenvalue analysis of the T-matrix. Assuming that T is a diagonalizable matrix, which is generally the case, we can write the eigenvalue equation

$$\mathbf{T} \cdot \mathbf{q}_i = \lambda_i \mathbf{q}_i \tag{2.17}$$

or

$$T \cdot Q = \Lambda \cdot Q \tag{2.18}$$

where Q is the N×N matrix with columns being the normalized eigenvectors of T while Λ is the diagonal matrix consisting of the eigenvalues. By assumption, T possesses a full set of independent eigenvectors and T is well conditioned enough so that the eigenvalues and eigenvectors can be extracted. The real parts of λ_i are all negative since the system probability must tend to zero at long

times if the network is connected. The eigenvalues and eigenvectors of T represent the transient modes of the network with absorbing boundary conditions. The eigenvectors are different from those for the matrix G which defines steady state. The waiting time PDF, eq. (2.6), is then

$$f(t) = -\sum_{k} \left(\sum_{j} \sum_{i} Q_{ik} Q_{kj}^{-1} P_{j}(0) \right) \lambda_{k} e^{\lambda_{k} t} = -\sum_{k} c_{k} \lambda_{k} e^{\lambda_{k} t}$$
(2.19)

with

$$c_k = \sum_{j} \sum_{i} Q_{ik} Q_{kj}^{-1} P_j(0)$$
 (2.20)

where Q^{-1} is the inverse of Q. Equation (2.19) immediately yields

$$\langle t \rangle = -\sum_{k=1}^{N} \frac{c_k}{\lambda_k} \tag{2.21}$$

and

$$\langle t^2 \rangle = 2 \sum_{k=1}^{N} \frac{c_k}{\lambda_k^2} \tag{2.22}$$

with the randomness parameter given by

$$r = \frac{2\sum_{k} \frac{c_{k}}{\lambda_{k}^{2}} - \left(\sum_{k} \frac{c_{k}}{\lambda_{k}}\right)^{2}}{\left(\sum_{k} \frac{c_{k}}{\lambda_{k}}\right)^{2}}$$
(2.23)

If it happens that a single eigenvalue dominates the behavior, i.e., that $|\lambda_1|$ is much closer to zero than the remaining N-1 eigenvalues, then $r\rightarrow 1$ and the process is nearly Poisson. Under most circumstances, it is the lowest absolute eigenvalue that would then dominate the expansion of TOF and r. In that limit, normalization of f(t) gives $c_I=1$ which then implies that the TOF is just $v=|\lambda_1|$ and r=1 and thus the kinetics is dominated by a single bottleneck characterized by one eigenvalue. When more eigenvalues contribute, the coefficients must also be calculated which reflects the distribution of initial probability over the various eigenmodes of decay.

The eigenmodes of T physically correspond to pure decay modes in the manifold of transient states. Thus, we expect at long times that an initial probability distribution will approach

$$\mathbf{P}(t) \xrightarrow[t \gg \frac{1}{|\lambda_2|}]{} const \times \mathbf{q}_1 \cdot e^{\lambda_1 t}$$
 (2.24)

If the contribution of the q_I mode is subtracted off from P(t), then the q_2 becomes dominant in the remainder and so forth. This simple analysis overlooks how the actual initial probability distribution overlaps the eigenvectors as represented by the coefficients c_k , eq. (2.20). For the SMK simulation, P(0) will be a normalized distribution over the AS, and for many problems this corresponds to $P_i(0) = \delta_{i,1}$. It is possible, however, that the overlap of q_I with P(0) is extremely small so that a higher term dominates in the expansion. For the TOF, the key quantity that identifies the dominant term is the ratio $\frac{c_k}{\lambda_k}$. Interestingly, for the randomness parameter r we have two different quantities of importance, $\frac{c_k}{\lambda_k}$ and $\frac{c_j}{\lambda_j^2}$. It is possible that two distinct eigenvalues dominate in the < t> and < t> terms. It is seen that this case can yield very large values of r when $\frac{c_j}{\lambda_j^2} \gg \left(\frac{c_k}{\lambda_k}\right)^2$ and then that $r \to \frac{c_j}{c_k^2} \cdot \frac{\lambda_k^2}{\lambda_j^2} - 1$.

F. Sensitivity Analysis

To connect the eigenvalue value analysis of T-matrix to the energy picture of the catalytic cycles, it is necessary to relate the λ_i 's and q_i 's to the free energies of the barriers and wells chemical network. The explicit formula for T of eq. (2.5) does this but that does not provide much insight or schemes to simplify the mechanism. Instead, we identify the key barriers and wells that control the eigenvalues using sensitivity analysis 65 66 closely related to the degree of reaction control. Thus, we can compute numerical sensitivity indices using

$$s_{i,j} = \frac{\partial \ln(|\lambda_i|)}{\partial \Delta G_i}$$
 (2.25)

where ΔG_j are well and barrier energies. In this way we identify which barriers and wells are controlling each eigenvalue. Consider an example where a single pathway dominates the rate, and the dominant lowest eigenvalue is well separated from the others. In this case, the energy span

model applies and the sensitivity indices are only appreciable for two terms, the HTS and the LINT, i.e.,

$$s_{1,HTS} = -\frac{1}{k_B T} \tag{2.26}$$

$$s_{1,LINT} = \frac{1}{k_B T} \tag{2.27}$$

and is exponentially small for all other barriers and wells. Hence, if the sensitivity coefficients are computed numerically for a complicated mechanism via eq. (2.25), the observation of dominant negative/positive pairs ($s_{1,HTS}$, $s_{1,LINT}$) suggests a reaction route that includes that pair. If the sensitivity analysis reveals more than one contributing pair of important coefficients, then a multiple pathway mechanism is indicated. Most importantly, however, the sensitivity analysis points to the parts of mechanism that require the most accurate treatment and improvement. We find that many of the higher eigenvalues can also be related to unique pairs of eigenvalues, i.e., $|\lambda_i| \approx \frac{k_B T}{h} exp \left[-\frac{(\Delta G_{barrier,i} - \Delta G_{well,i})}{k_B T} \right]$ for certain other pairs of states in the network identified by the analog of eqs. (2.26) and (2.27).

III. Examples

To illustrate the use of the eigenvalue analysis, we consider several examples of increasing complexity. The first is the classic linear catalytic chain with a single active site and a single product. This example exhibits the anticipated behavior where the TOF and the randomness parameter are dominated by the lowest eigenvalue. Furthermore, the energetic span theory is confirmed by the sensitivity analysis which associates the highest activation energy with the lowest eigenvalue. The second example consists of two parallel catalytic cycles coupled at a single active site. The case chosen illustrates that the smallest absolute eigenvalue may no longer control the TOF. Instead, the reactive flux follows the pathway of "least resistance" which can follow the second lowest eigenvalue for certain parameter ranges. Unlike for the linear chain, the randomness parameter for this case can exceed unity if appreciable flux is distributed over both paths. The energetic span theory is successfully generalized by including two barriers and one well as in eq. (2.16). Finally, we consider the case of a realistic catalytic system, based on the hydrogenation reaction of styrene on a SAC of vanadium. 67-69 This example shows three intertwined reaction

routes, three AS, two substrates, an inhibitor, and a structural disorder parameter that affects all the barriers and wells in the system. Despite the complexity of this model, we find that the eigenvalue analysis combined with sensitivity analysis sorts out the reaction paths controlling the observable TOF and r.

A. Linear cycles of length N

For a conventional single linear pathway catalytic cycle, as in Fig. 1a, the behavior of the TOF and the randomness parameter is straightforward. We form the T-matrix for a catalytic cycle with N sequential reaction steps as the tridiagonal expression involving the forward and backward rates, r_j and b_j respectively, where b_N =0. As an illustration, we choose an N=8 cycle with barrier and well free energies given in Fig. 1b and a substrate concentration set at [S]=1 M. The initial state, in this case, is simply $P_0 = (1,0,0,0,0,0,0,0)^T$ since there is a single active site. As a continuous parameter, we vary the well energy of the 4^{th} intermediate in units of $k_B T$, ϵ =E_{X4}, over the range from -10 to 1 while the remainder of the network remains unaltered. The value of $k_B T$ is set to 0.5 and the rate is expressed in units of $k_B T/h$.

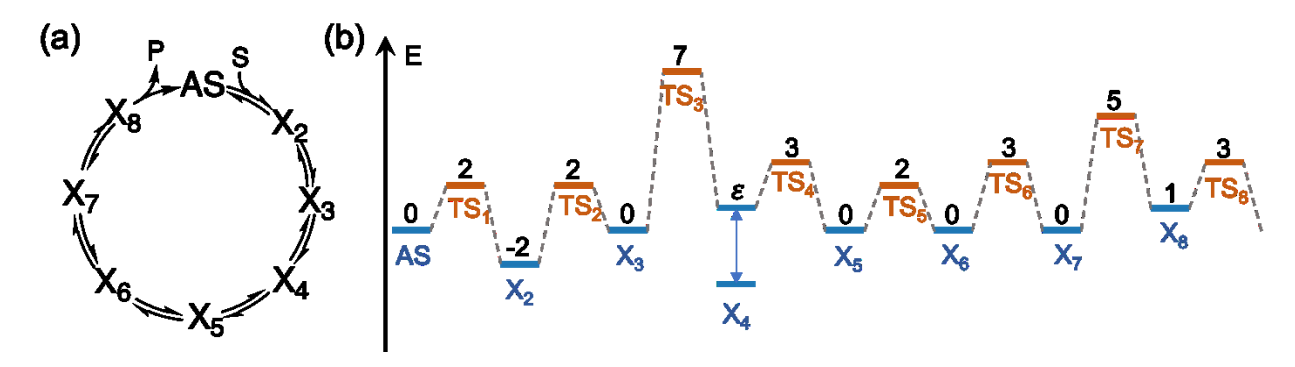


Fig. 1. The linear cycle with eight species and eight reactions. In (a), the cycle is depicted showing that X_1 is the active site following the observed product release. In (b) the energies chosen for the barriers and wells where the well energy of X_4 is called ε and allowed to vary.

In the energetic picture, a jump occurs at ε =-4 where the controlling features of the catalytic network abruptly change. For ε <-4, the LINT is X₄ and the HTS is TS₇. For ε >-4, the LINT is X₂ and the HTS is TS₄. Furthermore, we note that the activation energy is constant for ε > -4, E_a =9, while for ε < -4 we have E_a =9-(ε +4). The eigenvalue spectrum versus ε is shown in Fig. 2a along with the exact value of the TOF indicated with a dashed line. The two smallest eigenvalues are seen to undergo an avoided crossing very near ε = -4. The *T*-matrix remains diagonalizable even

near the avoided crossing although the two eigenvectors do become close in direction. The exact TOF follows closely the lowest eigenvalue, $|\lambda_1|$, and only exhibits visible deviations near the avoided crossing region. At the point $\epsilon = -4$ the randomness parameter r minimizes as seen in Fig. 2c. To improve the representation near $\epsilon = -4$, we can include the lowest two eigenvalues,

$$\frac{1}{\nu} \approx -\frac{c_1}{\lambda_1} - \frac{c_2}{\lambda_2} \qquad (3.1)$$

where the coefficients are obtained from eq. (2.20); eq. (3.1) is also plotted in Fig. 2a. As seen in the expanded view, Fig. 2b, this approximation eliminates most of the error in both ν and r. Likewise, we can expand the full PDF f(t), in terms of the eigenvalue expansion via

$$f(t) \approx -c_1 \lambda_1 e^{\lambda_1 t} - c_2 \lambda_2 e^{\lambda_2 t} \qquad (3.2)$$

which gives excellent agreement with the exact expression even at the avoided crossing.

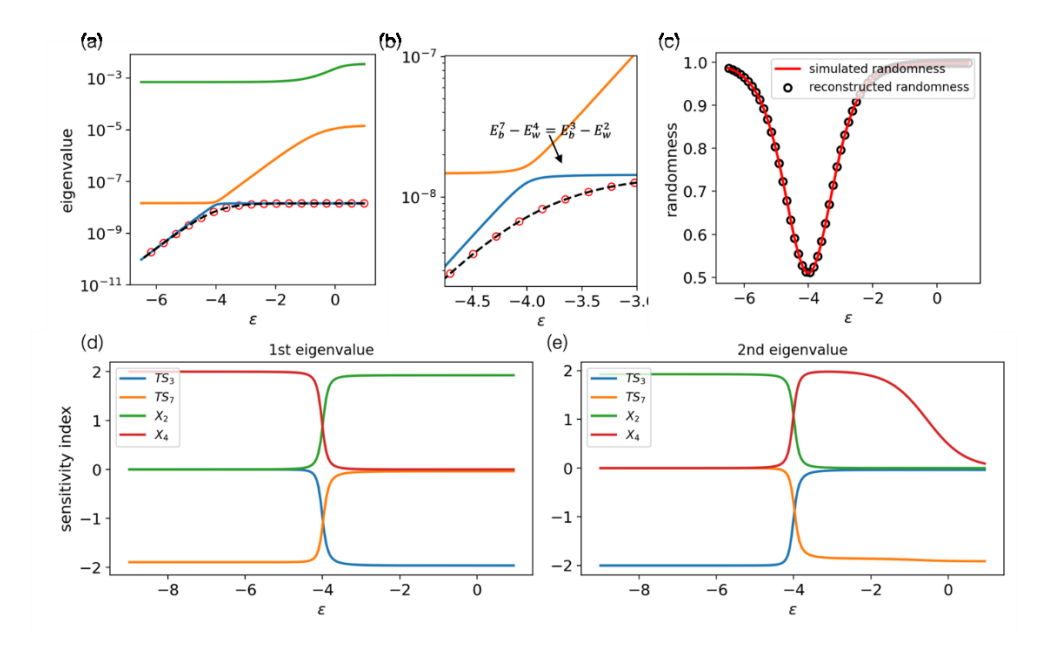


Fig. 2 Numerical application of the eigenvalue method to an eight species linear cycle. In (a) the lowest three absolute eigenvalues of T are plotted versus the well depth of X_4 , ε . The TOF from eq. (2.8) is seen follow the lowest absolute eigenvalue except near the avoided crossing at ε =-4. The two term reconstruction of the TOF eq. 3.1 is shown in (a) and, in greater detail, in (b). In (c) the randomness parameter versus ε is shown along with the two term reconstruction. In (d) and (e) the largest sensitivity indices of the lowest two eigenvalues with respect to the barrier and well energies are plotted versus ε .

The controlling structures for this simple linear pathway problem can be directly guessed from the energetic span theory. It is useful, however, to demonstrate that they can be also recovered from sensitivity analysis of the *T*-matrix. The sensitivity indices of the two lowest eigenvalues,

 $s_{i,j} = \frac{\partial ln|\lambda_i|}{\partial \Delta E_j}$, versus the parameter ε are shown in Fig. 2d and 2e. The index for the lowest eigenvalue, i=1, shown in Fig. 2d, is seen to be most sensitive to is X_4 and TS_7 for $\varepsilon < -4$. For $\varepsilon > -4$ it is most sensitive to X_2 and TS_4 . Interestingly, we see that the sensitivity of the second lowest eigenvalue exhibits precisely the reverse of this behavior. The numerical value of $s_{i,j}$ for the sensitive structures are seen to be ± 2 , consistent which the predictions of eqs. (2.26) and (2.27), while $s_{i,j}$ for the other structures are small. The sensitivity analysis thus correctly identifies the HTS and LINT and explains the change in the global rate flux pattern versus continuously changing parameters. It also helps identify the physical meaning of these two eigenmodes of T. Consider a "diabatic construction" where the eigenvalues are allowed to cross at ε =-4. One mode, with a constant eigenvalue corresponding to E_a =9 everywhere in ε , describes the flux as a most probable state X_2 across the bottleneck TS_4 . The other diabatic state crosses the first at ε =-4 with a constant slope and corresponds to flux from the most probable (variable energy) state X_4 with TS_7 being the flux bottleneck.

B. Multiple Pathways: Two Coupled Parallel Cycles

A simple multipath catalytic system consists of two N=4 cycles coupled at the active site, thus having seven species and eight reactions, i.e.

$$AS + P_B \underset{k_{4B}}{\longleftarrow} B_3 \underset{k_{\pm 3B}}{\longleftrightarrow} B_2 \underset{k_{\pm 2B}}{\longleftrightarrow} B_1 \underset{k_{\pm 1B}}{\longleftrightarrow} AS + S \underset{k_{\pm 1A}}{\longleftrightarrow} A_1 \underset{k_{\pm 2A}}{\longleftrightarrow} A_2 \underset{k_{\pm 3A}}{\longleftrightarrow} A_3 \underset{k_{4A}}{\longleftrightarrow} AS + P_A$$

A schematic of the reaction is shown in Fig. 3a and the energies used are shown in Fig. 3b. The probability vector is labeled according to $(AS, A_1, A_2, A_3, B_1, B_2, B_3)$ with the initial state $P_0 = (1,0,0,0,0,0,0,0)^T$. The product producing steps, $A_3 \underset{k_{4a}}{\longrightarrow} AS + P_B$ and $B_3 \underset{k_{4b}}{\longrightarrow} AS + P_B$, are irreversible and signify the end of the event time and the beginning of a new cycle. Hence, f(t) is the distribution of waiting times regardless of the product identity, P_A or P_B . The T-matrix is 7×7 in this case and is easily constructed from the mechanism using TST from the well and barrier energies. The reaction may proceed along either along with pathway A or B with a branching ratio given explicitly by $(\tau_A^T \cdot T^{-1} \cdot P_0) : (\tau_B^T \cdot T^{-1} \cdot P_0)$ where τ_A and τ_B are the absorption vectors into product states of the A and B cycles. Assigning a particular event to a given pathway is not cleancut since it is possible for a molecule to backtrack from one path to the other before the final

irreversible step to an absorbing state. This is a general characteristic of multi-pathway systems. We investigate the behavior of the system as the energy of the barrier $\varepsilon = \Delta E_{TSA2}^0$ is raised continuously from 3 to 10. From the energetic profile, shown in Fig. 3b, we expect the process to proceed along path A for low values of ε , where $\Delta E_{TSA4}^0 = 6$ is the rate limiting barrier, and then will switch to path B when $\Delta E_{TSB4}^0 = \varepsilon$ is the rate limiting barrier at high ε . The crossing point should be at $\varepsilon = 7$. Notice the activation energy goes from $E_a = 8$ at low ε to $E_a = 7$ at high ε . The objective here is to illustrate how the spectral analysis of the T-matrix reveals the pathway behavior.

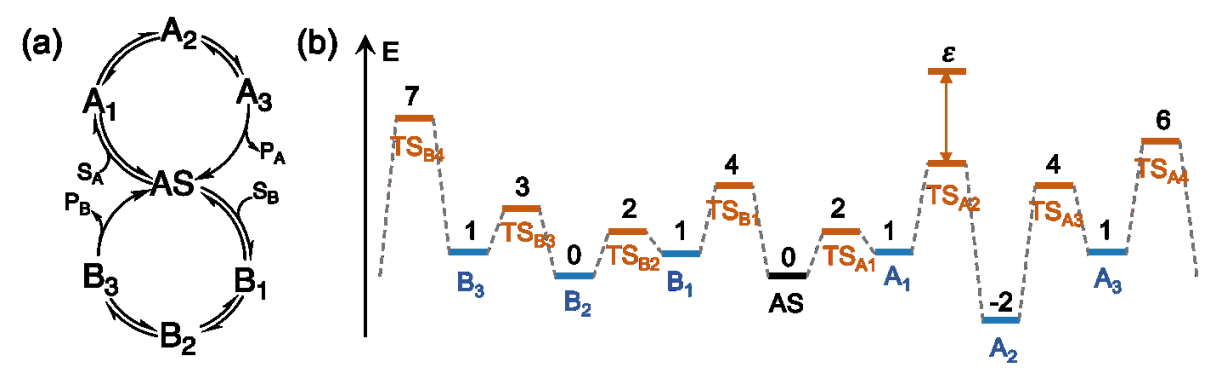


Fig. 3 The parallel two path catalytic cycle. In (a) we show a schematic diagram of the reaction mechanism where a single active site can catalyze a reaction along two independent pathways leading to two distinct products, P_A and P_B . In (b) we show the energetic profile chosen for the numerical study where the barrier for reaction $A_1 \rightarrow A_2$ is selected as the independent variable ε .

In Fig. 4a we show the lowest three eigenvalues of T as a function of the barrier height ε along with the exact TOF carried out at $k_BT=0.25$ using time units of h/k_BT with unit substrate concentrations. From this correlation diagram, it is seen that the lowest pair of eigenvalues undergo a broad avoided crossing around $\varepsilon=7$ where the highest transition state barriers cross, i.e., for reactions r_{A2} and r_{B4} . We see that λ_I is nearly flat while λ_2 shows most of the curvature associated with the crossing. Interestingly, the exact TOF, shown with the dashed line, effectively switches from the lowest eigenvalue (at small ε) to the second lowest eigenvalue (at large ε). This eigenvalue switching behavior is very accurately reproduced by a two term expansion of the TOF, eq. (3.2), which is also shown in Fig. 4a. It is worth noting that the coefficient for the lowest eigenvalue, c_I , approaches zero at high ε and one at low ε , while c_2 behaves oppositely since $c_I+c_2\approx I$. At the same time that the coefficients c_I and c_2 are undergoing switching, the branching ratio goes from dominantly A selective to dominantly B selective, shown in Fig. 4c. Mathematically, the explanation of the eigenvalue switching phenomena of the TOF relates back to the definition, $v = \frac{1}{1^T \cdot (-T)^{-1} \cdot P_0}$. The projection of the eigenvector unto the initial state P_0

determines the coefficients c_i ; the c_I is very small at large ε since its eigenvector has a vanishing small projection onto the initial state. The eigenvectors represent pure exponential decay modes within the manifold of transient states and the modes need not involve the AS strongly.

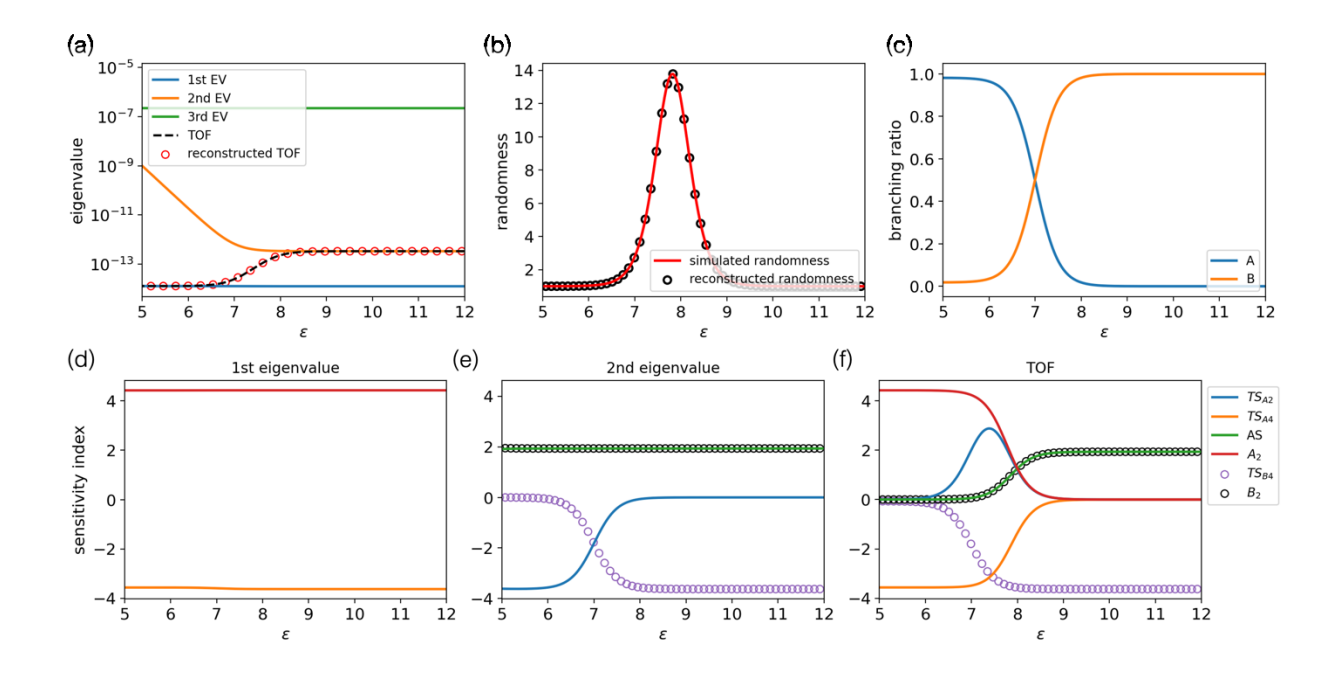


Fig. 4. Numerical application of the eigenvalue method to the two parallel path model system represented in Fig. 3. In (a) the lowest three absolute eigenvalues of T are plotted versus the barrier height TS_{A2} , ε . The TOF from eq. (2.7) is seen to resemble the lowest absolute eigenvalue below ε =7 whereafter it smoothly switches to resembling the second lowest eigenvalue. A two term reconstruction of the TOF is also shown in (a) and is very close to the exact TOF. In (b) the randomness parameter versus ε is shown along with its term reconstruction. In (c) the branching fraction into the A and B paths is plotted versus ε . In (d) and (e) the largest sensitivity indices of the lowest two eigenvalues with respect to the barrier and well free energies are plotted versus ε . In (f) the sensitivity indices of the full TOF are shown.

The physical basis of the eigenvalue switching is revealed by a sensitivity analysis of the barriers and wells. In Fig. 4f, we show the sensitivity index of the full TOF for the most important barrier and well energies. The indices are positive for well energies and negative for barrier energies. It is seen that at low ε the TOF is most sensitive to the well energy for A₂ and the barrier energy for TS_{A4}. At high ε , the TOF is most sensitive to the wells AS and B₂ (which have equal energy and split the $1/k_BT$ sensitivity evenly between them) and to barrier TS_{B4}. Near the switching point, ε =7, there is a narrow region of positive sensitivity to barrier TS_{A2}. Clearly as the barrier for TS_{A2} increases, the flux switches from the A path (where TS_{B4} is the HTS and A₂ is the LINT) to the B path (where TS and B₂ are co-LINT's and TS_{B4} is the HTS). The eigenvalue analysis gives a clearer picture. As illustrated in Fig. 4d, the smallest absolute eigenvalue | λ_1 | shows sensitivity

to barrier TS_{A4} and well A_2 for all ε . The eigenvector shows the highest probability for well A_2 and its decay flux passes dominantly over the barrier TS_{A4} . This behavior determines the TOF for low ε since $v\approx |\lambda_1|$ for ε <7. The second smallest eigenvalue shows the greatest sensitivity to the equivalent wells AS and B_2 for all ε values. However, the barriers sensitivity of switches from TS_{A2} for low ε to TS_{B4} at for high ε . This second eigenmode remains mostly located in the AS and B_2 wells, but flux direction changes near ε =7, i.e. pathway switching. Thus, the two eigenmodes of T are seen to reflect the most probable resting sites and the two reaction pathways available in this system. It may not always be the case that the eigenmodes clearly separate along chemical pathways, but it often occurs. It does seem always the case that the flux pattern within the manifold of transient states does change abruptly at a sharp avoided crossing.

Finally, we discuss the randomness parameter r as a function of ε . In Fig. 4b we see a tall peak in r vs. ε slightly above the point of avoided crossing. We see that r becomes greater than 1 during the avoided crossing, signifying a narrowing of the PDF f(t). The two mode expansion of r gives a mathematical explanation of this behavior. From eq. (2.23) we have

$$r \approx \frac{\frac{2c_1}{\lambda_1^2} + \frac{2c_2}{\lambda_2^2} - \left(\frac{c_1}{\lambda_1} + \frac{c_2}{\lambda_2}\right)^2}{\left(\frac{c_1}{\lambda_1} + \frac{c_2}{\lambda_2}\right)^2}$$
(3.4)

In the present case, the two eigenvalues are roughly constant versus ε over the interesting region from ε =7-9 with $\lambda_2 \approx 25\lambda_1$. Since the normalization of f(t) demands that $c_1 + c_2 = 1$, we can conclude that r will go up to about $r \sim \frac{1}{2} \frac{\lambda_2}{\lambda_1}$ when $c_1 \sim \frac{\lambda_1}{\lambda_2}$ in rough agreement with Fig. 4b which shows a maximum of $r \sim 14$. Physically, r > 1 here corresponds to multiple pathway contributions.

The TOF is well approximated in this problem is described by the generalization of the energetic span model that was presented in eq. (2.16). That model included two barriers going to distinct product channels, the HTSL and HTSR, along with a single LINT that is bracketed by the HTSL and HTSR. In the present case, at low ε the HTSL is TS_{B4}, the HTSR is TS_{A4}, and the LINT is A₂ which gives an activation energy of E_a =8. At high ε the HTSL is TS_{B4}, the HTSR is TS_{A2}, and the co-LINT's are AS and B₁ which gives an activation energy of E_a =7. The TOF is controlled by E_a , i.e. $\nu \approx \frac{kT}{h} \frac{1}{\sigma} e^{-\Delta E_a/kT}$ where σ is a symmetry number for the number of equivalent LINT's

or HTS's, or equal activation energies. In contrast, the parameter r is controlled by two activation energies in regions where non-Poisson statistics apply and thus is more informative.

C. Styrene Hydrogenation by a Single Atom Catalyst With Static Disorder

The analysis of realistic catalytic problems can be much more challenging than the model systems considered above and must be investigated without preconceived notions about the kinetics. As an illustration of the use of the eigenvalue method for an experimentally motivated example, we consider the styrene hydrogenation kinetics on an organovanadium SAC for which a microkinetic model was developed in a previous study. 70 71 The system consists of single V(III) atoms anchored to an amorphous silica support, assumed to be statically disordered, in contact with styrene (ST), H₂, and tetrahydrofuran (THF) in a nonpolar solution phase. The hydrogenation reaction, styrene+H2→ethylbenzene, is mediated by three active sites, here denoted by C, D, and E. The THF is present in the precatalyst and thereafter plays the role of an inhibitor. The active sites correspond to three distinct ligand arrangements around the vanadium atom and can interconvert by reversible attachment reactions from the solution. Each active site supports a catalytic cycle, here denoted by path 5, path 6, and path 7 for consistency with previous work¹⁰. As shown in the schematic of Fig. 5a, the cycles are coupled both through the interconversion of active sites and through shared steps of the different cycles. The free energy surface for the mechanism was obtained using DFT calculations. A representative free energy landscape for a particular choice of the disorder parameter is shown in Fig. 5b.

The DFT calculations of the free energies for the full catalytic network were obtained explicitly as a function of the local disorder. The present work expands on the supported organovanadium(III) catalyst model presented in our previous studies¹⁰ ⁷¹ by introducing an additional disorder parameter beyond the V-O(siloxane) distance (rvo), for site heterogeneity. This parameter is the Euclidean O-O bond distance (roo) between the two O atoms on the silica surface excluding the siloxane donor, which can be changed by increasing the O-V-O bond angle. As the Euclidean O-O bond distance on the surface has been shown to influence spectral features of X-ray absorption spectra for the pre-catalyst model,⁷² this dimension is considered in tandem with the V-O bond length. To generate the free energy surfaces for all intermediates and transition states shown in Fig. 5, a 5x5 grid of structures was generated using the V-O(siloxane) bond distance of 2.1, 2.2, 2.3, 2.4, and 2.5 Å and the O-O bond distance of 3.0, 3.3, 3.6, 3.9, and 4.2 Å. These

distances were chosen to adequately represent the effect of the donor siloxane and the surface grafting site heterogeneity, respectively. Further details are in the supporting information.

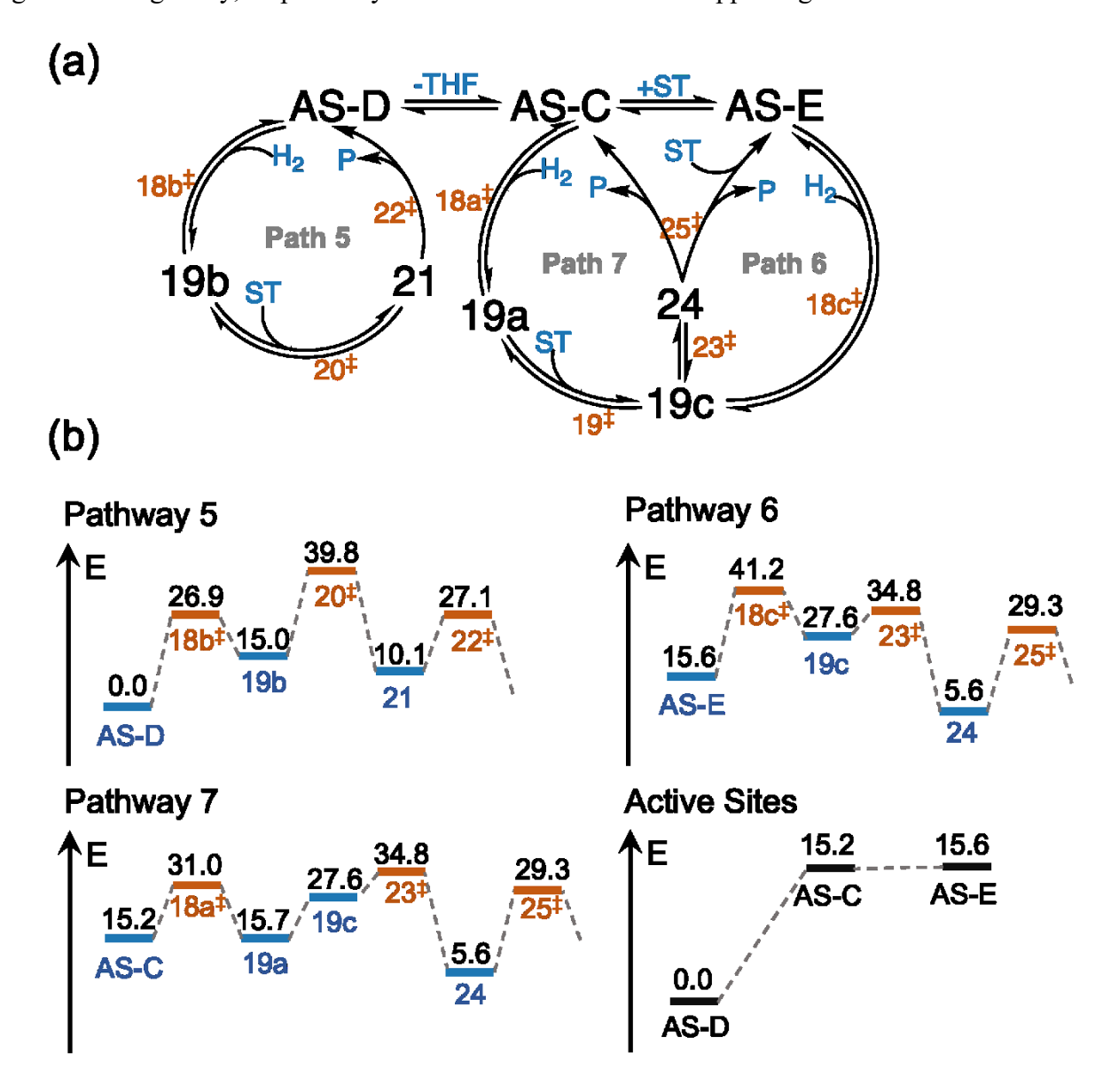


Fig. 5 The catalytic mechanism for $ST+H_2 \rightarrow ethylbenzene$ on a SAC. In (a) we show a schematic diagram of the reaction mechanism. There are three distinct pathways and three active sites. In (b) we show the free energy profile in kcal/mol along the pathway assuming the energy of AS-D is 0. The relative ordering of the AS's is shown in the final panel of (b). The disorder parameters are set to $r_{vo}=2.3$ Å and $r_{oo}=3.0$ Å. The other details of the model are described in ref. 10 and 65 and the supporting information.

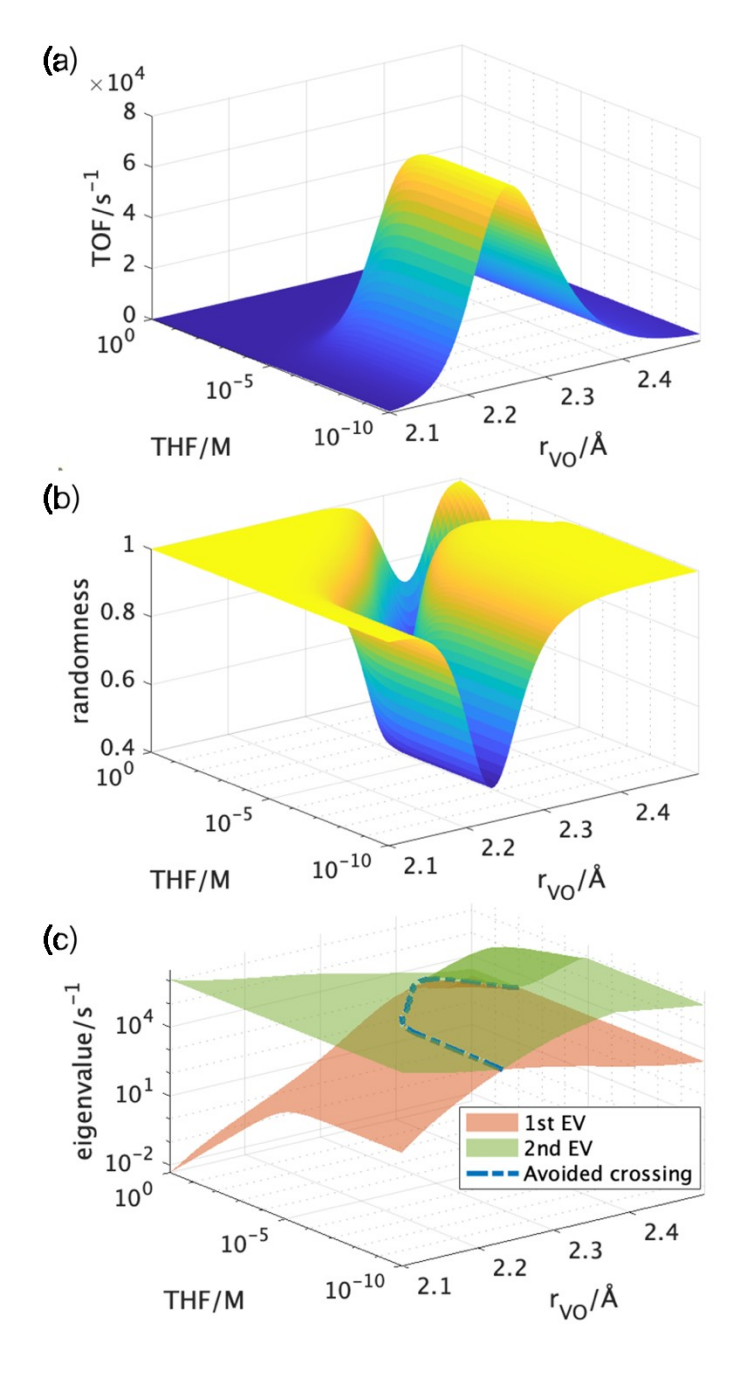


Fig. 6 Exact simulation results for $ST+H_2 \rightarrow ethylbenzene$ reaction on the vanadium based SAC. The results are computed for the special case of $r_{00}=3.0$ Å, [ST]=1 M, $[H_2]=5$ M, and T=600K. In (a) the TOF in s^{-1} is computed using eq. (2.7) where the inverse matrix T^{-1} is found using the INV command from MATLAB. In (b) the randomness parameter is computed from the matrix inverse. In (c) the lowest two eigenvalues are plotted obtained using the MATLAB command EIG and the location of the avoided crossing is shown with the dashed line which is close to the minimum trough seen in r.

The catalytic chemistry is parameterized by three continuous concentrations, [ST], [H₂], and [THF], and two continuous structural disorder parameters r_{VO} and r_{OO} . Since it is impossible to visualize the five-dimensional behavior of the full kinetics, we restrict our analysis here to the effect of two of these variables, r_{VO} and [THF] and the other parameters (r_{OO} , [H₂],[ST]) are fixed. The [THF] variable controls the distribution of active sites through the attachment reaction of THF and hence only one barrier of the mechanism is affected. On the other hand, r_{VO} affects the stability

of every barrier and well in the full chemical network. In Fig. 6a we show surface representation of the TOF versus (r_{VO} ,[THF]). In Fig. 6b the randomness parameter is plotted. In Fig. 6c the lowest two absolute eigenvalues of T are shown together with the smallest two absolute eigenvalues. The DFT calculations were carried out on a uniform two-dimensional grid in the structural parameters (r_{VO} , r_{OO}) and evaluated at the desired coordinate values using a tensor cubic spline interpolator. The results shown in Fig. 6 were obtained using the INV and EIG routines of the MATLAB suite. We find that TOF obtained using the general expression eq. (2.7) lies very close to the smallest absolute eigenvalue, $v \approx |\lambda_1|$ everywhere except very near the points of eigenvalue avoided crossing where $|\lambda_1(r_{VO},[THF])| \approx |\lambda_2(r_{VO},[THF])|$. We also see a pronounced ridge in $v(r_{VO},[THF])$ that describe optimal values of the TOF. The randomness parameter shows a pronounced trough with a 90° elbow occurring in the (r_{VO} , THF]) plane that matches the position of the avoided crossing seen in Fig. 6c. The plateau region of r lies near r=1 while minimum of the through lies near the value r=0.5.

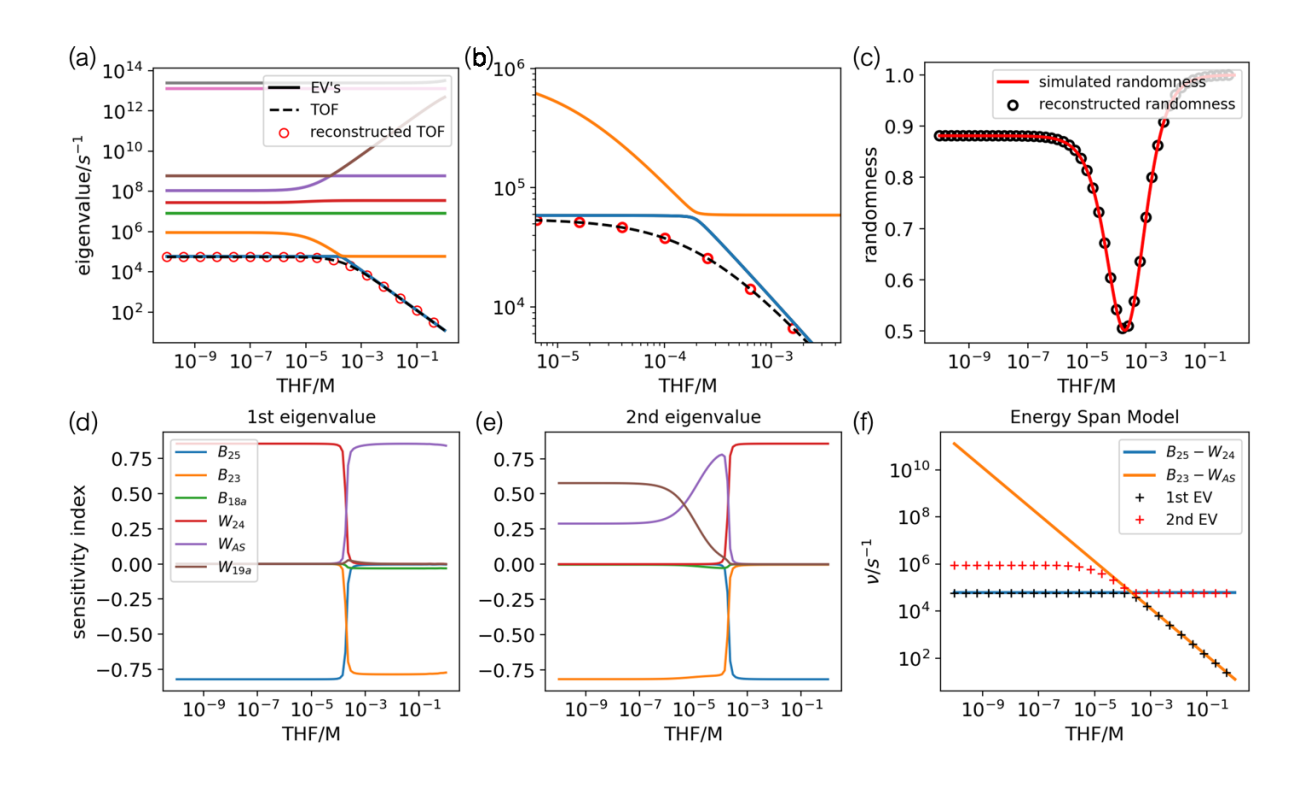


Fig. 7. Numerical application of the eigenvalue method to the vanadium SAC system represented in Fig. 5 taken as a function of [THF] at rvo=2.3Å. In (a) the absolute eigenvalues of T are plotted versus the [THF] in M units. The TOF from eq. (2.8) is seen following the lowest absolute eigenvalue for all concentrations of THF. The small deviation of the TOF from $|\lambda_1|$ is modeled accurately by the two term expansion seen in (b). A two term of the TOF is also shown in (a) and is very close to the exact TOF. In (c) the randomness parameter versus ε is shown along with the two term reconstruction. In (c) the branching fraction into the A

and B paths is plotted **versus** ε . In (d) and (e) the largest sensitivity indices of the lowest two eigenvalues with respect to the barrier and well energies are plotted versus ε . In (f) the prediction of the energetic span theory is shown with solid lines for two choices of HTS and LINT along with the two lowest eigenvalues. The eigenvalues are well modeled by the energetic span theory.

To obtain a more detailed view of the kinetic behavior of this system, we look at several one-dimensional cuts of the functions $v(r_{VO}[THF])$ and $r(r_{VO}[THF])$ holding one of the arguments fixed. In Fig. 7, we show the results as a function of [THF] at r_{VO} =2.3 Å. It should be borne in mind that the THF concentration effectively stabilizes the active site AS-D (i.e. V-THF) by a factor of $k_BT \cdot \ln[THF]$ and changes the free energy barrier for AS-D \rightarrow AS-C by negative a similar factor. The energies of the other structures in the model are unaffected by variations in [THF]. In Fig. 7a, we show the eigenvalue spectrum along with the TOF. We see that many of the eigenvalues are nearly constant versus [THF], however, the lowest two absolute eigenvalues show a sharp avoid crossing near [THF]=2×10⁻⁴ M. One other pair of much larger eigenvalues similarly undergoes avoided crossing at that point. The exact TOF mirrors the lowest eigenvalue except in the vicinity of the avoided crossing. As seen in the expanded view of the crossing region, Fig. 7b, the TOF nearly perfectly coincides with the two term reconstruction given by eq. (3.2). The randomness parameter exhibits a minimum r≈0.52 at THF value slightly above the avoid crossing but yet completely consistent with the two eigenvalue formula eq. (3.4). Interestingly, r does not asymptote to 1 at low [THF] but goes to about $r\approx 0.88$. This reflects the numerical proximity of the lowest two eigenvalues and is predicted accurately by formula (3.2).

A second slice of $v(r_{VO}, [THF])$ and $r(r_{VO}, [THF])$ is made as a function of r_{VO} at $[THF]=10^{-7}\,\mathrm{M}$ which is summarized in Fig. 8. In Fig. 8a we show the eigenvalue spectrum and the TOF versus r_{VO} . Since the structural variable r_{VO} affects all the barriers and wells in the mechanism, the eigenvalues exhibit a much more intricate dependence on r_{VO} than previously seen for [THF]. Again, however, the most important feature is an avoided crossing of the lowest two absolute eigenvalues at $r_{VO}=2.23\,\mathrm{Å}$. The exact TOF, shown with a dashed line, closely follows $|\lambda_1|$ except very near the avoided crossing while the two term expansion for the TOF, eq. (3.2), very closely approximates the exact answer even there as seen in the expanded view presented in Fig. 8b. The randomness parameter, presented in Fig. 8c, minimizes at r=0.5 at a slightly larger value of r_{VO} than the crossing of the eigenvalues. The two term expansion of r, eq. (3.4), accurately represents its behavior. The other avoided crossings seen in Fig. 8a involving higher eigenvalues in the spectrum have little influence on the observables TOF and r. Physically, the corresponding higher

eigenmodes describe rapid relaxation processes within the manifold of transient states that quickly damp out as the system approaches steady state.

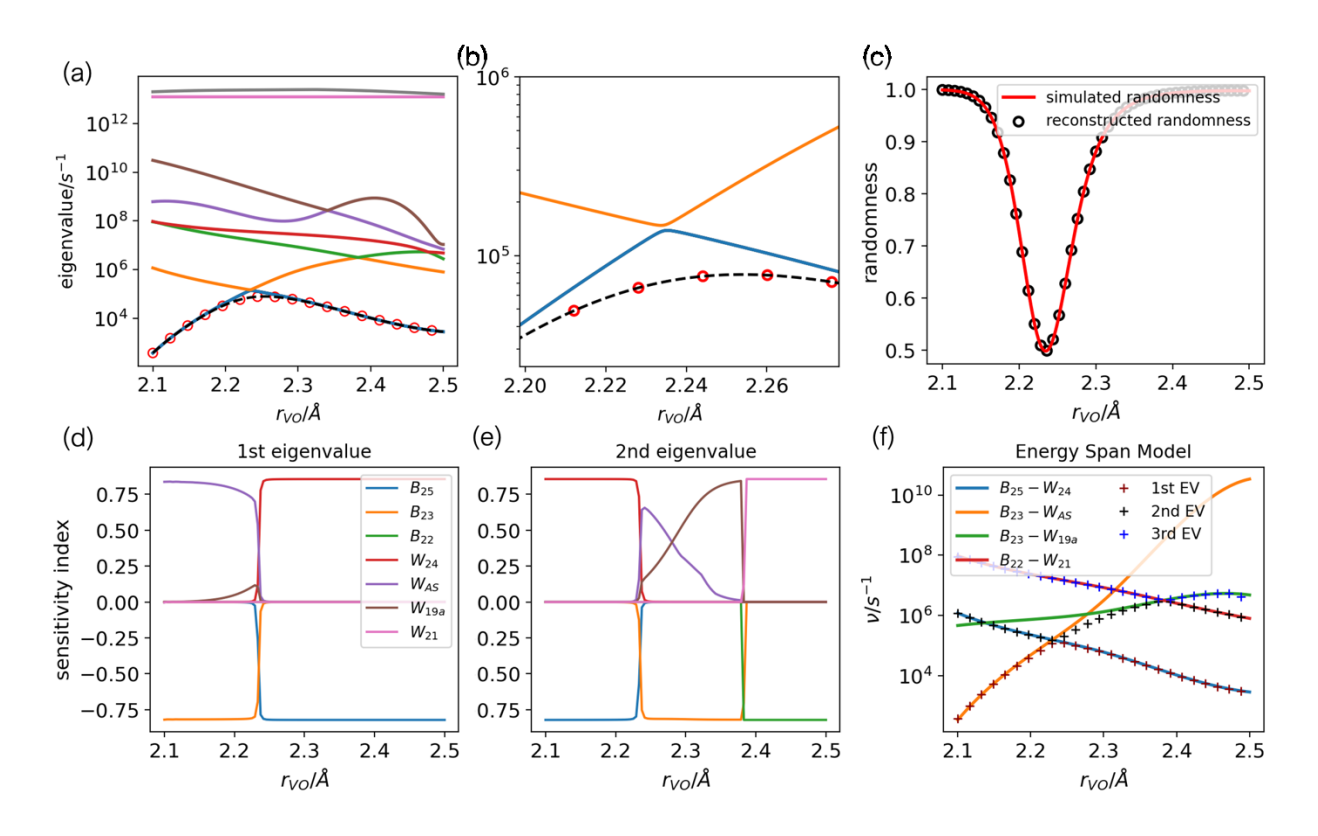


Fig. 8. Numerical application of the eigenvalue method to the vanadium SAC system represented in Fig. 3 taken as a function of r_{VO} at $[THF]=10^{-7}$ M. In (a) the absolute eigenvalues of T are plotted versus rvo. The TOF from eq. (2.8) is seen to follow the lowest absolute eigenvalue for all rvo. The small deviation of the TOF from $|\lambda_1|$ near the avoided crossing is modeled accurately by the two term expansion seen in (b). In (c) the exact randomness parameter versus rvo is shown along with the two term reconstruction. In (d) and (e) the largest sensitivity indices of the lowest two eigenvalues with respect to the barrier and well energies are plotted versus rvo. In (f) the prediction of the energetic span theory is shown with solid lines for four choices of HTS and LINT along with the three lowest eigenvalues.

Finally, we use sensitivity analysis to determine the pathways and key steps that control the catalytic kinetics shown in Figs. 7 and 8. In Fig. 7d, we show the largest sensitivity indices of the wells (positive) and barriers (negative) for $|\lambda_1|$ versus [THF] at r_{VO} =2.3Å. We see an abrupt transition occurring at [THF]=2×10⁻⁴ M where the avoided crossing between $|\lambda_1|$ and $|\lambda_2|$ occurs. At low [THF], $|\lambda_1|$ is sensitive to well 24 and barrier 25[†] (see Fig. 5a) corresponding to adjacent states along pathway 7. For high [THF], $|\lambda_1|$ becomes sensitive to the active sites AS-C and AS-D and to the barrier 23[†]. We note that the pair of active sites lie in a quasi-equilibrium since the process V+THF \rightarrow V-THF is barrierless, and thus their sensitivity moves in tandem. These sensitivity steps correspond to a non-sequential configuration along pathway 7. The sensitivity of

 $|\lambda_2|$, Fig. 7e, shows the reverse of this process, thus being sensitive to wells AS-C and -D and barrier 23[†] below the crossing and to 24 and 25[†] above the crossing. We note that for very low [THF] values the $|\lambda_2|$ begins to interact with higher eigenvalues adding further sensitivity to other structures. However, for the determination of the TOF and r, the two pairs are sufficient to explain the results.

The sensitivity analysis identifies a clear LINT and HTS pair along a reaction pathway that can be used to predict the overall TOF. Specifically, we know that energetic span theory of single path reactions predicts $k(T) \approx \frac{kT}{h} \exp(-(\Delta G_{HTS} - \Delta G_{LINT})/kT)$. In Fig. 7f, we use two possible pairings (HTS,LINT)=(25[†],24) and (23[†],AS-D) to compute the TOF from this energetic span approximation; these are shown with the two solid lines. The exact eigenvalues are shown with dashed lines. It is seen that the energetic span theory is a very accurate representation of $|\lambda_1|$ everywhere except very close to the avoided crossing and as is $|\lambda_2|$. However, the energetic span theory gives a diabatic representation of the eigenvalues allowing them to actually cross and retain their identification with specific structures. Since the TOF $\sim |\lambda_1|$ corresponds to adiabatic avoided crossing the energetic span theory requires redefinition of HTS and LINT at the avoided crossing. The analysis thus reveals that the reaction is dominated by a single reaction pathway for all [THF] although the structures determine the activation energy change versus [THF]. Furthermore, the randomness parameter never rises above 1 and shows a minimum at 0.5 when the two activation barriers become equal $\Delta G_{HST}^{23} - \Delta G_{LINT}^{AS-C/E} = \Delta G_{HST}^{25} - \Delta G_{LINT}^{24}$ corresponding to two TS's acting sequentially. Pathway 7 shown in Fig. 5a is clearly dominant in the kinetics and the [THF] dependence reflects the change in the rate limiting process as the free energy barrier for V-THF→V+THF is systematically altered.

A similar sensitivity analysis has been carried out for Fig 8, the r_{VO} coordinate. In Fig. 8d $|\lambda_1|$ is seen most sensitive to barrier 25[†] and to well 24 above the avoided crossing with $|\lambda_2|$, $r_{VO}>2.23$ Å. Below the crossing, it is most sensitive to barrier 23[†] and to well AS-C. The second lowest eigenvalue $|\lambda_2|$ shows the reverse of this behavior. Interestingly, $|\lambda_2|$ also shows a second abrupt transition occurring near $r_{VO}=2.38$ Å where $|\lambda_2|$ and $|\lambda_3|$ undergo avoided crossing. The structures involved there are barrier 22[†] and well 21 with the barrier 23[†] and well 19a. The analysis again suggests a single pathway dominates the TOF chemistry, pathway 7 from Fig. 5, but the

controlling structures along with that path change as a function of r_{VO} . We again applied the energetic span model using the three pairs of (HTS, LINT) structures identified by the sensitivity analysis with one additional pairing included for comparison. In Fig. 8f, the approximation $|\lambda| \approx \frac{kT}{h} \exp(-(\Delta G_{HTS} - \Delta G_{LINT})/kT)$ is seen to be a good representation of the $|\lambda_1|$, $|\lambda_2|$ and $|\lambda_3|$ in the relevant ranges of r_{VO} . In particular, it closely matches $|\lambda_1|$ which models the TOF. It is quite interesting that the energetic span theory can be applied with some accuracy to higher eigenvalues which goes beyond the initial formulation of the theory.

IV. Conclusions

We have found that the single molecule view of catalysis that emphasizes the waiting time distribution between product formation events has yielded new insight into the general catalytic kinetics which may be of use in the analysis of SAC. In particular, we found that an eigenvalue decomposition of the transition matrix, T, can explain a variety of behaviors of both the TOF and the randomness parameter observables. The advantage of the spectral approach is that the kinetics can be decomposed into a hierarchy of timescales. The longest times, i.e. the smallest $|\lambda|$, often yields the TOF for the network. The next longest time allows us to compute the randomness parameter. The third longest timescale gives the skew of the PDF, f(t). The challenge to the experimentalist is to extract trajectory data over a wide enough range to accurately extract the timescales. Like all kinetics problems, the slowest timescale process is rate limiting and the most important. Faster processes rapidly go quickly into steady state and are harder to observe. The spectral decomposition allows the cleanest separation of these processes.

The relationship between the eigenvalues of T and the energetic structure of the chemical network was revealed clearly through a conventional sensitivity analysis. The eigenvalues were shown to be related to specific barriers and wells along the dominant reaction pathways that could be quantified using the energetic span method, i.e $|\lambda_i| \approx \frac{k_B T}{h} \cdot \exp\left(-\left(\Delta G_{HTST}^i - \Delta G_{LINT}^i\right)/k_B T\right)$ which reflects rate limiting barriers and most stable points along chemical pathways. It is obvious that such expressions develop because of the cancelation of common terms in effective rate expressions along the chemical pathway. What is exciting about the present analysis is that the higher eigenvalues also seem to satisfy this formula. Can an energetic span theory be developed for the higher moments of f(t) and hence the randomness parameter itself? This question is under

investigation. We have found that the observable quantities in the SAC experiment are generally

responsive to two eigenvalues of the transition matrix, and in turn, those eigenvalues are controlled

by a few key barriers and wells in the catalytic network. Therefore, we expect that a reasonable

mechanism improvement strategy would involve more extensive calculations of the free energies

that focus on those structures. The points at which r exhibits minima or maxima versus a

controllable parameter are usually associated with avoided crossings of eigenvalues. Those

avoided crossings were demonstrated to correlate with the crossing of activation energies

somewhere in the network. This behavior could signal the change in the HTS or LINT along a

single path or even the switching of the pathway itself.⁷³

Acknowledgements

This work was supported by the National Science Foundation through grant CHE1664555. This

work was also supported by the U.S. Department of Energy (DOE) Office of Basic Energy

Sciences, Division of Chemical Sciences, Geosciences, and Biosciences, Catalysis Science

Program under Contract DE-AC02-06CH11357 (Argonne National Laboratory). All DFT

calculations were performed using the computational resources provided by the Laboratory

Computing Resource Center (LCRC) at Argonne National Laboratory (ANL).

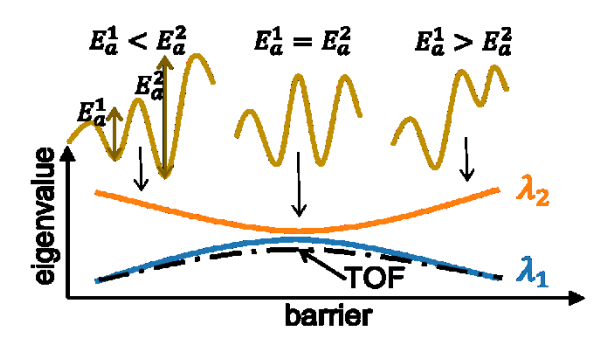
Author Information

Corresponding author for kinetics: rex.skodje@colorado.edu

Corresponding author for DFT: congliu@anl.gov

27

TOC-graphic



Supporting Information: Includes the structural information about the DFT calculations.

References

-

¹ Stamatakis, M.; Chen, Y.; Vlachos, D. G. First-Principles-Based Kinetic Monte Carlo Simulation of the Structure Sensitivity of the Water-Gas Shift Reaction on Platinum Surfaces. *J. Phys. Chem. C* **2011**, *115* (50), 24750–24762.

² Holby, E. F.; Wu, G.; Zelenay, P.; Taylor, C. D. Structure of Fe-Nx-C Defects in Oxygen Reduction Reaction Catalysts from First-Principles Modeling. *J. Phys. Chem. C* **2014**, *118* (26), 14388–14393.

³ Li, H.; Evans, E. J.; Mullins, C. B.; Henkelman, G. Ethanol Decomposition on Pd-Au Alloy Catalysts. *J. Phys. Chem. C* **2018**, *122* (38), 22024–22032.

⁴ Bray, J. M.; Schneider, W. F. First-Principles Analysis of Structure Sensitivity in NO Oxidation on Pt. *ACS Catal.* **2015**, *5* (2), 1087–1099.

⁵ Thomas, J. M. The Societal Significance of Catalysis and the Growing Practical Importance of Single-Site Heterogeneous Catalysts. In *Proceedings of the Royal Society A: Mathematical, Physical and Engineering Sciences*; **2012**; *468* (2143), 1884–1903.

⁶ Zhang, Z.; Su, J.; Matias, A. S.; Gordon, M.; Liu, Y. S.; Guo, J.; Song, C.; Dun, C.; Prendergast, D.; Somorjai, G. A.; *et al.* Enhanced and Stabilized Hydrogen Production from Methanol by Ultrasmall Ni Nanoclusters Immobilized on Defect-Rich h-BN Nanosheets. *Proc. Natl. Acad. Sci. U. S. A.* **2020**, *117* (47), 29442–29452.

⁷ Goldsmith, B. R.; Peters, B.; Johnson, J. K.; Gates, B. C.; Scott, S. L. Beyond Ordered Materials: Understanding Catalytic Sites on Amorphous Solids. *ACS Catal.* **2017**, *7* (11), 7543–7557.

⁸ Boudart, M.; Djéga-Mariadassou, G. *Kinetics of heterogeneous catalytic reactions*; Princeton University Press: Princeton, NJ, 2014.

⁹ Wang, Y. -G.; Mei, D.; Glezabou, V. -A.; Li, J.; Rousseau, R. Dynamic formation of single-atom catalytic active sites on ceria-supported gold nanoparticles. *Nat. Commun.* **2015**, *6* (1), 6511.

¹⁰ Wells, R. H.; An, S.; Patel, P.; Liu, C.; Skodje, R. T. Single-Molecule Kinetics of Styrene Hydrogenation on Silica-Supported Vanadium: The Role of Disorder for Single-Atom Catalysts, *J. Phys. Chem. C*, **2021**, *125* (37), 20286-20300.

¹¹ Moerner, W. E.; Kador, L. Optical Detection and Spectroscopy of Single Molecules in a Solid. *Phys. Rev. Lett.* **1989**, *62* (21), 2535–2538.

¹² Moerner, W. E.; Fromm, D. P. Methods of Single-Molecule Fluorescence Spectroscopy and Microscopy. *Review of Scientific Instruments* **2003**, 74 (8), 3597–3619.

¹³ Komatsuzaki, T.; Kawakami, M.; Takahashi, S.; Yang, H.; Silbey, R. J. *Single-Molecule Biophysics: Experiment and Theory*, Vol. 146; John Wiley & Sons: Hoboken, NJ, 2012.

¹⁴ Cornish, P. V.; Ha, T. A Survey of Single-Molecule Techniques in Chemical Biology. *ACS Chemical Biology* **2007**, *2* (1), 53–61.

¹⁵ Lu, H. P.; Xun, L.; Xie, X. S. Single-Molecule Enzymatic Dynamics. *Science* **1998**, 282 (5395), 1877–1882.

- ¹⁶ Schnitzer, M. J.; Block, S. M. Statistical Kinetics of Processive Enzymes. *Cold Spring Harbor Symp. Quant. Biol.* **1995**, *60*, 793–802.
- ¹⁷ Shaevitz, J. W.; Block, S. M.; Schnitzer, M. J. Statistical Kinetics of Macromolecular Dynamics. *Biophys. J.* **2005**, 89 (4), 2277–2285.
- ¹⁸ English, B. P.; Min, W.; Van Oijen, A. M.; Kang, T. L.; Luo, G.; Sun, H.; Cherayil, B. J.; Kou, S. C.; Xie, X. S. Ever-Fluctuating Single Enzyme Molecules: Michaelis-Menten Equation Revisited. *Nat. Chem. Biol.* **2006**, *2* (2), 87–94
- ¹⁹ Kou, S. C.; Cherayil, B. J.; Min, W.; English, B. P.; Xie, X. S. Single-Molecule Michaelis-Menten Equations. **2005**. *109* (41), 19068-19081.
- ²⁰ Chemla, Y. R.; Moffitt, J. R.; Bustamante, C. Exact Solutions for Kinetic Models of Macromolecular Dynamics. *J. Phys. Chem. B* **2008**, *112* (19), 6025–6044.
- ²¹ Moffitt, J. R.; Bustamante, C. Extracting signal from noise: kinetic mechanisms from a Michaelis–Menten-like expression for enzymatic fluctuations. *FEBS J.* **2014**, *281*, 498–517.
- ²² Cao, J.; Silbey, R. J. Generic Schemes for Single-Molecule Kinetics. 1: Self-Consistent Pathway Solutions for Renewal Processes. *J. Phys. Chem. B* **2008**, *112* (41), 12867–12880.
- ²³ Cao, J. Michaelis-Menten Equation and Detailed Balance in Enzymatic Networks. *J. Phys. Chem. B* **2011**, *115* (18), 5493–5498.
- ²⁴ Ninio, J. Alternative to the Steady-State Method: Derivation of Reaction Rates from First-Passage Times and Pathway Probabilities. *Proc. Natl. Acad. Sci. U. S. A.* **1987**, *84* (3), 663–667.
- ²⁵ Ge, H.; Qian, M.; Qian, H. Stochastic Theory of Nonequilibrium Steady States. Part II: Applications in Chemical Biophysics. *Physics Reports* **2012**, *510* (3), 87–118.
- ²⁶ Wu, J.; Cao, J. Generalized Michaelis-Menten Equation for Conformational Modulated Monomeric Enzymes. *Adv. Chem. Phys.* **2011**, *146*, 329-366.
- ²⁷ Xu, W.; Kong, J. S.; Yeh, Y. T. E.; Chen, P. Single-Molecule Nanocatalysis Reveals Heterogeneous Reaction Pathways and Catalyticdynamics. *Nat. Mater.* **2008**, *7* (12), 992–996.
- ²⁸ Chen, P.; Zhou, X.; Shen, H.; Andoy, N. M.; Choudhary, E.; Han, K.-S.; Liu, G.; Meng, W. Single-molecule fluorescence imaging of nanocatalytic processes. *Chem. Soc. Rev.* **2010**, *39* (12), 4560–4570.
- ²⁹ Han, K. S.; Liu, G.; Zhou, X.; Medina, R. E.; Chen, P. How Does a Single Pt Nanocatalyst Behave in Two Different Reactions? A Single-Molecule Study. *Nano Lett.* **2012**, *12* (3), 1253–1259.
- ³⁰ Andoy, N. M.; Zhou, X.; Choudhary, E.; Shen, H.; Liu, G.; Chen, P. Single-Molecule Catalysis Mapping Quantifies Site-Specific Activity and Uncovers Radial Activity Gradient on Single 2D Nanocrystals. *J. Am. Chem. Soc.* **2013**, *135* (5), 1845–1852.
- ³¹ Shen, H.; Zhou, X.; Zou, N.; Chen, P. Single-Molecule Kinetics Reveals a Hidden Surface Reaction Intermediate in Single-Nanoparticle Catalysis. *J. Phys. Chem. C* **2014**, *118* (46), 26902–26911.
- ³² Ye, R.; Mao, X.; Sun, X.; Chen, P. Analogy between Enzyme and Nanoparticle Catalysis: A Single-Molecule Perspective. *ACS Catal.* **2019**, *9* (3), 1985–1992.
- ³³ Chen, T.; Dong, B.; Chen, K.; Zhao, F.; Cheng, X.; Ma, C.; Lee, S.; Zhang, P.; Kang, S. H.; Ha, J. W.; *et al.* Optical Super-Resolution Imaging of Surface Reactions. *Chem. Rev.* **2017**, 117, 7510–7537.
- ³⁴ Buurmans, I. L. C.; Weckhuysen, B. M. Heterogeneities of individual catalyst particles in space and time as monitored by spectroscopy. *Nat. Chem.* **2012**, *4*, 873–886.
- ³⁵ Roeffaers, M. B. J.; Sels, B.F.; Uji-I, H.; De Schryver, F. C.; Jacobs, P. A.; De Vos, D. E.; Hofkens, J. Spatially resolved observation of crystal-face dependent catalysis by single turnover counting. *Nature* **2006**, *439* (7076), 572–575.
- ³⁶ Tachikawa, T.; Yamashita, S.; Majima, T. Evidence for Crystal-Face-Dependent TiO₂ Photocatalysis from Single-Molecule Imaging and Kinetic Analysis, *J. Am. Chem. Soc.* **2011**, *133*, 7197-7204.
- ³⁷ Xu, W.; Kong, J.S.; Chen P. Single-molecule kinetic theory of heterogeneous and enzyme catalysis. *J. Phys. Chem. C* **2009**, *113*(6), 2393–2404.
- ³⁸ Gillespie, D. T. Markov Processes: An Introduction for Physical Scientists; Academic Press: San Diego, 1992.
- ³⁹ Qian, H.; Elson, E. L. Single-Molecule Enzymology: Stochastic Michaelis–Menten Kinetics. *Biophys. Chem.* **2002**, *101*, 565-576.
- ⁴⁰ Neuts, M. F. *Matrix-geometric solutions An algorithmic approach*; The Johns Hopkins University Press: Baltimore, MD, 1981.
- ⁴¹ Liebovitch, L. S.; Toth, T. I. Distributions of activation energy barriers that produce stretched exponential probability distributions for the time spent in each state of the two state reaction A≠B. *Bull. Math. Biol.* **1991**, *53* (3), 443-455
- ⁴² Efros, A. L.; Nesbitt, D. J. Origin and control of blinking in quantum dots, *Nature Nanotech* **2016**, *16*, 661-671.

- ⁴³ Moffitt, J. R.; Chemla, Y. R.; Bustamante, C. Mechanistic constraints from the substrate concentration dependence of enzymatic fluctuations. *Proc. Natl. Acad. Sci.* **2010**, *107* (36), 15739–15744.
- ⁴⁴ Jung, W.; Yang, S.; Sung, J. Novel chemical kinetics for a single enzyme reaction: relationship between substrate concentration and the second moment of enzyme reaction time. *J. Phys. Chem. B* **2010**, *114*, 9840–9847.
- ⁴⁵ Yang, S.; Cao, J.; Silbey, R. J.; Sung, J. Quantitative interpretation of the randomness in single enzyme turnover times. *Biophys J.* **2011**, *101*, 519–524.
- ⁴⁶ Chaudhury, S.; Cao, J.; Sinitsyn, N. A. Universality of Poisson Indicator and Fano Factor of Transport Event Statistics in Ion Channels and Enzyme Kinetics. *J. Phys. Chem. B* **2013**, *117*, 503–509.
- ⁴⁷ Kramer, Z. C.; Gu, X. K.; Zhou, D. Y.; Li, W. X.; Skodje, R. T. Following molecules through reactive networks: Surface catalyzed decomposition of methanol on Pd (111), Pt (111), and Ni (111). *J. Phys. Chem. C* **2014**, 118, 12364–12383.
- ⁴⁸ Sabatino, A.; Frezzato, D. Tagged-moiety viewpoint of chemical reaction networks. *J. Chem. Phys.*, **2019**, *150*, Article no. 134104.
- ⁴⁹ Bai, S.; Zhou, D. Y.; Davis, M. J.; Skodje, R. T. Sum over histories representation of chemical kinetics. *J. Chem. Phys. Lett.* **2015**, *6*, 183-188.
- ⁵⁰ Bai, S.; Davis, M. J.; Skodje, R. T. Sum over histories representation for kinetic sensitivity analysis: How chemical pathways change when reaction rate coefficients are varied, *J. Phys. Chem. A* **2015**, *119*, 11039-11052.
- ⁵¹ Frezzato, D. Sensitivity analysis of the reaction occurrence and recurrence times in steady-state biochemical networks. *Mathematical Biosciences* **2021**, *332*, 108518.
- ⁵² Amatore C.; Jutand A. Mechanistic and kinetic studies of palladium catalytic systems. *J. Organomet. Chem.* **1999**, *576*, 254–278.
- ⁵³ Campbell, C. T. The Degree of Rate Control: A Powerful Tool for Catalysis Research. *ACS Catal.* **2017**, 2770–2779.
- ⁵⁴ Foscato, M.; Jensen, V. R. Automated in Silico Design of Homogeneous Catalysts. *ACS Catal.* **2020**, *10*, 2354–2377.
- ⁵⁵ Briggs, G. E.; Haldane, J. B. S. A Note on the Kinetics of Enzyme Action. *Biochem. J.* 1925, 19 (2), 338–339.
- ⁵⁶ Van Kampen, N. G. *Stochastic Processes in Physics and Chemistry*, 3rd ed.; Elsevier: Amsterdam, 2007.
- ⁵⁷ Berezhkovskii, A. M. Renewal Theory for Single-Molecule Systems with Multiple Reaction Channels. *J. Chem. Phys.* **2011**, *134*, 074114.
- ⁵⁸ Avila, T. R.; Piephoff, D. E.; Cao. J. Generic Schemes for Single-Molecule Kinetics. 2: Information Content of the Poisson Indicator. *J. Phys. Chem.* B **2017** (33), 7750-7760.
- ⁵⁹ Christiansen, J. A. The Elucidation of Reaction Mechanisms by the Method of Intermediates in Quasi-Stationary Concentrations. *Adv. Catal.* **1953**, *5*, 311.
- ⁶⁰ Cornish-Bowden, A. Fundamentals of Enzyme Kinetics; Portland Press Ltd.: London, 2004.
- ⁶¹ Amatore, C.; Jutand, A. Anionic Pd (0) and Pd (II) intermediates in palladium-catalyzed Heck and cross-coupling reactions. *Acc. Chem. Res.* **2000**, *33* (5), 314-321.
- ⁶² Kozuch, S.; Shaik, S. A Combined Kinetic-Quantum Mechanical Model for Assessment of Catalytic Cycles: Application to Cross-Coupling and Heck Reactions. *J. Am. Chem. Soc.* **2006**, *128* (10), 3355–3365.
- ⁶³ Kozuch, S.; Shaik, S. How to Conceptualize Catalytic Cycles? The Energetic Span Model, *Acc. Chem. Res.* **2011**, 44 (2), 101-110.
- ⁶⁴ Kozuch, S. A refinement of everyday thinking: the energetic span model for kinetic assessment of catalytic cycles. *WIREs: Comput. Mol. Sci.* **2012**, *2*, 795–815.
- ⁶⁵ Saltelli, A.; Ratto, M.; Andres, T.; Campolongo, F.; Cariboni, J.; Gatelli, D.; Sasana, M.; Tarantola, S. *Global Sensitivity Analysis. The Primer*; John Wiley & Sons: Hoboken, NJ, 2008.
- ⁶⁶ Zhou, D. Y.; Davis, M. J.; Skodje, R. T. Multitarget Global Sensitivity Analysis of N-Butanol Combustion. *J. Phys. Chem. A* **2013**, *117* (17), 3569–3584.
- ⁶⁷ Witzke, R. J.; Chapovetsky, A.; Conley, M. P.; Kaphan, D. M.; Delferro, M. Nontraditional Catalyst Supports in Surface Organometallic Chemistry. *ACS Catal.* **2020**, *10* (20), 11822–11840.
- ⁶⁸ Sohn, H.; Camacho-Bunquin, J.; Langeslay, R. R.; Ignacio-De Leon, P. A.; Niklas, J.; Poluektov, O. G.; Liu, C.; Connell, J. G.; Yang, D.; Kropf, J.; *et al.* Isolated, Well-Defined Organovanadium(III) on Silica: Single-Site Catalyst for Hydrogenation of Alkenes and Alkynes. *Chem. Commun.* **2017**, *53*, 7325–7328.
- ⁶⁹ Kaphan, D. M.; Ferrandon, M. S.; Langeslay, R. R.; Celik, G.; Wegener, E. C.; Liu, C.; Niklas, J.; Poluektov, O. G.; Delferro, M. Mechanistic Aspects of a Surface Organovanadium(III) Catalyst for Hydrocarbon Hydrogenation and Dehydrogenation. *ACS Catal.* **2019**, *9*, 11055–11066.

⁷¹ Patel, P.; Wells, R. H.; Kaphan, D.; Delferro, M.; Skodje, R. T.; Liu, C. Computational Investigation of the Role of Active Site Heterogeneity for a Supported Organovanadium(iii) Hydrogenation Catalyst. *ACS Catal.* **2021**, *11*, 7257-7269.

⁷⁰ Liu, C.; Camacho-Bunquin, J.; Ferrandon, M.; Savara, A.; Sohn, H.; Yang, D.; Kaphan, D. M.; Langeslay, R. R.; Ignacio-de Leon, P. A.; Liu, S.; *et al.* Development of Activity–Descriptor Relationships for Supported Metal Ion Hydrogenation Catalysts on Silica. *Polyhedron* **2018**, *152*, 73–83.

⁷² Patel, P.; Lu, Z.; Jafari, M. G.; Hernandez-Prieto, C.; Zatsepin, P.; Mindiola, D. J.; Kaphan, D. M.; Delferro, M.; Kropf, A. J.; Liu, C., Integrated Experimental and Computational K-edge XANES Analysis of Vanadium Catalysts. *ChemRxiv* **2022**, DOI: 10.26434/chemrxiv-2022-g1jqx-v2.

⁷³ Wells, R. H.; Skodje, R. T. Pathway-Switching Mechanism for Water-Catalyzed Ethanol Decomposition on Cu(111) *J. Phys. Chem. C* **2020**, *124* (17), 9385-9393.